nature photonics

Article

https://doi.org/10.1038/s41566-023-01295-w

Continuous wideband microwave-to-optical converter based on room-temperature Rydberg atoms

In the format provided by the authors and unedited

S.1 SUPPLEMENTARY DISCUSSION ON THE EFFICIENCY OF CONVERSION

The estimation of the efficiency of the microwave-to-optical conversion appears to be a complex topic if considered in free space. Most simulations predict optical photon rates [phot/s] for given MW intensities [W/m^2] (or equivalently [phot/s/m^2]). These are also the quantities directly available in the experiment, where the intensity can be obtained from the Autler-Townes splitting calibration, and the photon rates from the single photon counting. To arrive with the efficiency of the conversion, η [phot/phot], one has to perform a full 3D near-field simulation of the conversion process.

A simpler approach is to consider an effective aperture [m^2], where the conversion occurs. This is completely correct in the case of a large (larger than the wavelength) conversion medium. However, we operate in the subwavelength regime, $w_0 = 100\ \mu\text{m} \ll 21.5\ \text{mm} = \lambda_{\text{MW}}$, where this approach may lead to errors and a full near-field simulation would be more appropriate, especially in the case of significant conversion efficiency. In the case of great efficiency, the field is (by assumption) strongly affected by the ensemble, therefore significant diffraction may occur and thus the resulting effective area is larger than assumed. Nevertheless, the efficiency obtained from this approach will be the true photon-to-photon efficiency if the single-mode MW field is confined to the atomic medium volume, for example using a traveling-wave resonator/waveguide, but also with a cavity. In free space however, one needs to remember that a radiation mode cannot be confined to such a small volume, and therefore the given efficiency does not correspond to any free-space mode.

To achieve a proper comparison with the results of other groups, especially Ref. [33-35], we would like to perform a similar estimation of an effective aperture. However, it is important to note that our implementation differs from the ones in Ref. [33-35]. In these cases the interaction area is determined by cold atoms trapped in MOT, whose shape and optical density can be straightforwardly measured e.g. with camera imaging. On the other hand, in our case the interaction area is defined by three optical laser beams (Gaussian) interacting with atomic gas freely entering and exiting the area. Additionally, the conversion efficiency is in fact nontrivially position-dependent due to the beams' profiles, induced light shifts, and saturation effects.

Effective aperture

We undertake a simple approach similar to the Ref. [33-35] to estimate the effective interaction area, while stressing that as our overall efficiency is relatively small, we can neglect the diffraction effects along the atomic ensemble. In case of a single Gaussian beam with waist w_0, assuming conversion's linear dependence on the intensity of an optical field, I, one would arrive with effective area estimate at the focus of the beam

$$2\pi \int_0^\infty \exp\left(-\frac{2r^2}{w_0^2}\right) r\mathrm{d}r = \frac{1}{2}\pi w_0^2. \tag{1}$$

In our case, however, the process is driven by four transitions in Gaussian beams (the probe transition considered twice as in the Fig. 1**b**) of the same waist. In this case the effective area of relevant Gaussian product is

$$2\pi \int_0^\infty \left(\exp\left(-\frac{2r^2}{w_0^2}\right)\right)^4 r\mathrm{d}r = \frac{1}{8}\pi w_0^2. \tag{2}$$

Taking that estimate in the $w_0 = 100\ \mu$m case, with the measured peak results – photon rate $(4.44\pm0.08)\cdot10^5$ phot/s for MW intensity $(8.1\pm0.9)\cdot10^{-8}$ W/m^2 – leads us to the overall achieved peak conversion efficiency of 1.3±0.1%.

Losses in the experimental setup

The implemented setup is subject to losses in the output of the converter. We put the consideration of all the losses in the Sup. Tab. I. The measurements were performed with an assisting 776 nm field propagating along the expected conversion's direction. Overall losses account for 58%.

Accounting for losses in the setup leads us to an estimate of atomic peak conversion efficiency of 3.1±0.4%.

Theoretical estimate

To obtain a theoretical estimate of the efficiency of conversion, we perform numerical simulations in the context of the theory presented in the manuscript. Thus we interrogate the results of our full atomic simulation, as given

Source of loss	Loss percentage
exit window of the (uncoated) vapor cell	10%
optical filtering setup	19%
fiber coupling	16%
fiber-fiber connector	20%
photon detector	15%
overall loss	58%

Supplementary Table I. Analysis of losses at the output of the converter in the experimental setup.

by Eq. (1) in the $\partial_t \hat{\rho}(t) = 0$ case. Within the linear regime (as in the Fig. 2**a**) we check that at peak conversion we obtain the mapping from incident microwave Rabi frequency onto an output optical atomic coherence ρ_s, observing a slope $\beta = \mathrm{d}\rho_s/\mathrm{d}\Omega_{\mathrm{MW}} = 17\ (\mathrm{rad/s})^{-1} \approx 1.1 \times 10^{-4} (2\pi\mathrm{MHz})^{-1}$ (quantyfing amount of atomic coherence per unit of Rabi frequency). This allows us estimate an intensity-to-intensity efficiency as the ratio of microwave and optical field intensities normalized by the photon energy ratio. The expression is following, and in the linear regime:

$$\eta = \frac{\varepsilon_0 (\Omega_{\mathrm{MW}} \hbar / d_{\mathrm{MW}})^2}{\varepsilon_0 |\frac{ik_s}{2\varepsilon_0} n L_{\mathrm{eff}} d_s \rho_s|^2} \frac{\omega_{\mathrm{MW}}}{\omega_s} = \frac{(\hbar/d_{\mathrm{MW}})^2}{|\frac{ik_s}{2\varepsilon_0} n L_{\mathrm{eff}} d_s|^2} \beta^{-2} \frac{\omega_{\mathrm{MW}}}{\omega_s},$$

where the variables follow the convention introduced in the main text, and additionally $d_{\mathrm{MW}} = 2500 a_0 e$ and $d_s = 0.95 a_0 e$ are electric dipole moments of MW and *signal* transitions respectively (a_0 being Bohr radius and e being elementary charge), $n \approx 7{\cdot}10^{16}\ 1/\mathrm{m}^3$ is atomic number density and $L_{\mathrm{eff}} \approx 2.5$ cm is an effective interaction length. In the numerator we have the microwave field intensity obtained from the calibrated microwave Rabi frequency. In the denumerator we have the intensity of the optical field, under the assumption of uniform generation along the ensemble and no input signal depletion (which remains valid for low efficiencies). There are several parameters here that bear significant uncertainties, which leads to a rough estimate of $\eta = 2.8 \pm 1.6\%$, which agrees with the experimental result.

S.2 PHOTON RATES, NOISE LEVELS AND NOISE-EQUIVALENT TEMPERATURE

Cross-correlation analysis of laser fields

The values of various components of the observed optical signal have been obtained by a cross-correlation analysis based on measuring the output photon rate for all possible combinations of one or more lasers switched off. In the first step, the preliminary measurements identified the cross-correlation between all the introduced optical fields. Photons rates for all of the combinations of laser fields are presented in the Sup. Fig. 1. It was observed that the MW field had no effect on photon rates, apart from the obvious case with all the other fields on, where we observe the conversion of coherent state. To extract the information about each field contributing to the overall registered signal (i.e. in the p+c+d case), we treat the measured values (in the order from the Sup. Fig. 1) as a vector and perform a matrix operation on it with the inverse of the correlation matrix:

$$\begin{pmatrix} 1&0&0&0&0&0&0&0 \\ 1&1&0&0&0&0&0&0 \\ 1&0&1&0&0&0&0&0 \\ 1&0&0&1&0&0&0&0 \\ 1&1&1&0&1&0&0&0 \\ 1&1&0&1&0&1&0&0 \\ 1&0&1&1&0&0&1&0 \\ 1&1&1&1&1&1&1&1 \end{pmatrix}^{-1} = \begin{pmatrix} 1&0&0&0&0&0&0&0 \\ -1&1&0&0&0&0&0&0 \\ -1&0&1&0&0&0&0&0 \\ -1&0&0&1&0&0&0&0 \\ 1&-1&-1&0&1&0&0&0 \\ 1&-1&0&-1&0&1&0&0 \\ 1&0&-1&-1&0&0&1&0 \\ -1&1&1&1&-1&-1&-1&1 \end{pmatrix}. \tag{3}$$

This results in photon rate contributions for each combination of fields, which we present in the Sup. Fig. 2. We note that the contributions of two-field combinations are near-zero and thus we neglect them in further considerations. Furthermore, we interpret the p+c+d case as the thermal radiation coupling to the converter.

In the second step we modified the optical filtering setup of the converted signal (776 nm) in order to eliminate the effects of other lasers disturbing the photon counting measurements (cases p, c and d). Namely, we replaced

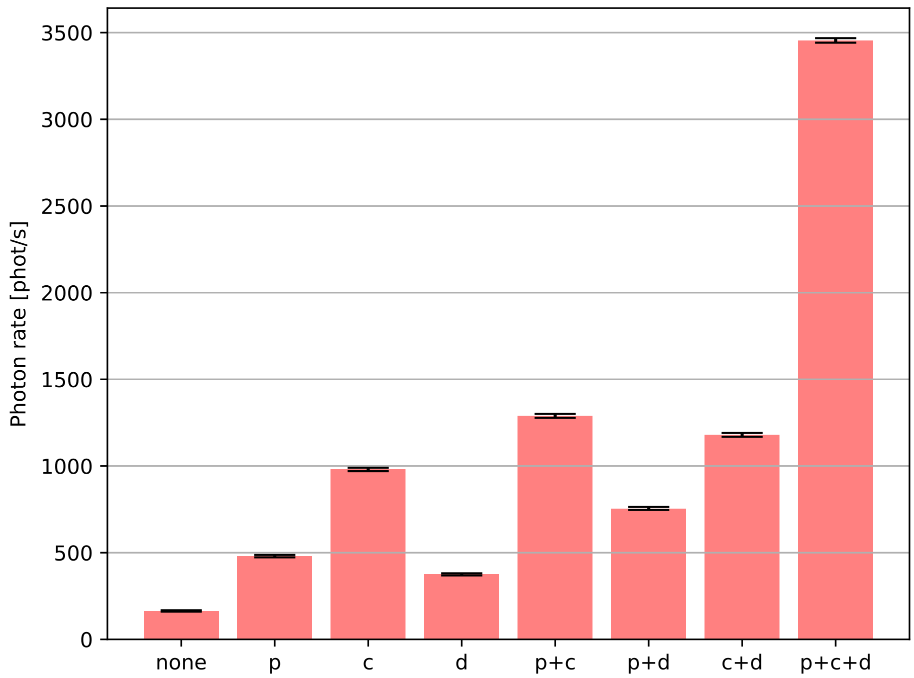

Supplementary Figure 1. Photon rates registered for each combination of fields before introducing spectral filters. p – *probe* (780 nm), c – *coupling* (480 nm), d – *decoupling* (1258 nm). The MW field has no effect on photon rates, apart from the case with all the other fields on. The error bars are calculated from photon-counting standard deviation, $\sqrt{\bar{n}}$, where in each case $\bar{n}$ is explicitly noted as photon rates on the Y axis.

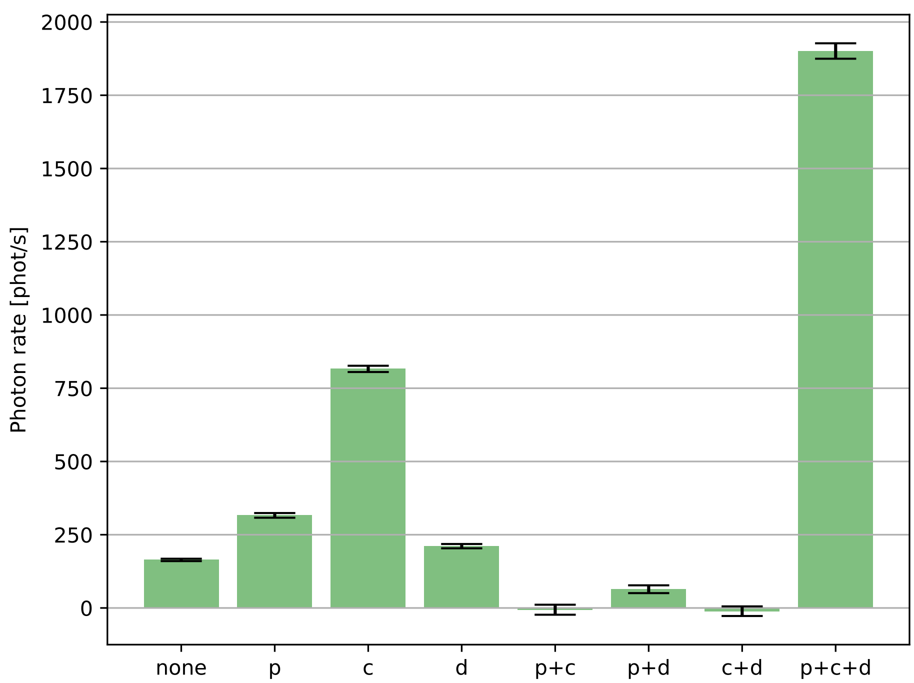

Supplementary Figure 2. Photon rate contributions for each combination of fields before introducing spectral filters. p – *probe* (780 nm), c – *coupling* (480 nm), d – *decoupling* (1258 nm). The MW field has no effect on photon rates, apart from the case with all the other fields on. The error bars are calculated from the propagation of the standard deviation from the Sup. Fig. 1, where in each case $\bar{n}$ is explicitly noted as photon rates on the Y axis.

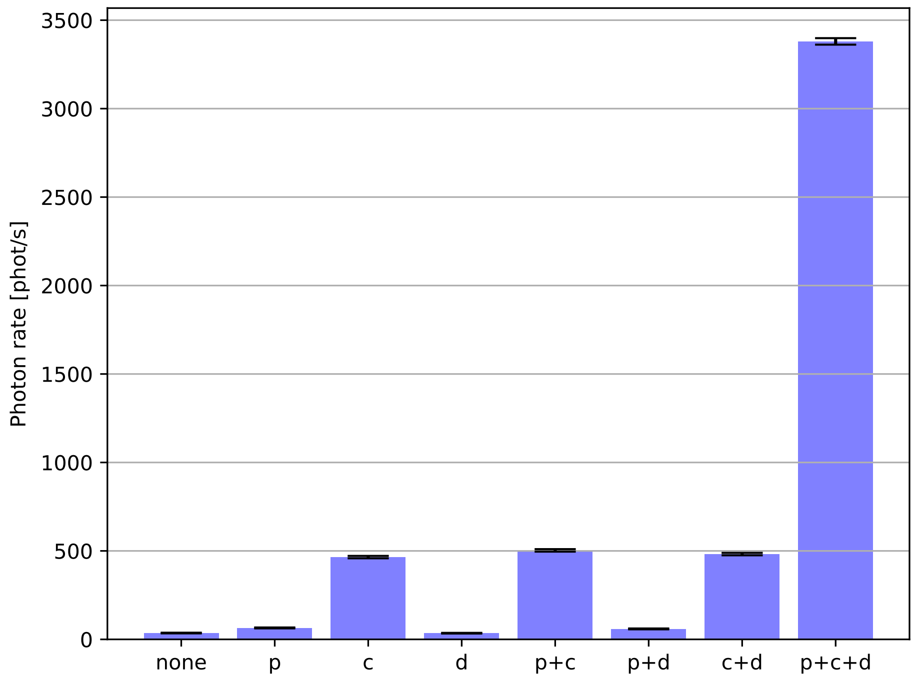

Supplementary Figure 3. Photon rates registered for each combination of fields after introducing spectral filters. *p* – *probe* (780 nm), *c* – *coupling* (480 nm), *d* – *decoupling* (1258 nm). Again, the MW field has no effect on photon rates, apart from the case with all the other fields on. The error bars are calculated from photon-counting standard deviation, $\sqrt{\bar{n}}$, where in each case $\bar{n}$ is explicitly noted as photon rates on the Y axis.

a 10 nm bandwidth filter used in the preliminary measurements with the set of filters described in the Methods (highpass, lowpass, 1.2 nm bandpass). This led to the registered rates in the Sup. Fig. 3 and the analysis has shown the elimination of photon rate contributions in the cases p and d, as shown in the Sup. Fig. 4. However, photon rate contribution in the case c could not be fully eliminated – we identify this effect as wideband fluorescence of glass elements induced by the 480 nm field. From now on to assess the fluorescence (and other) noise level, we turned off the 1258 nm field only. To assess the other noise level, we turned off the 480 nm field only.

In the third step, when measuring the dynamic range from the Fig. 2**a**, we measured photon rates of overall, thermal, fluorescence and other noise levels, as a reference. The results, consistent with the measurements in the main text, are presented in the Sup. Tab. II.

Noise-equivalent temperatures

The noise level (thermal and non-thermal) was measured in the $T = 300$K environment. We came to the conclusion that the ratio between thermal noise (measured if and only if every field was switched on) and non-thermal noise is 85% to 15%, as shown in the Sup. Fig. 4 and in the Sup. Tab. II. From that we deduce that the thermal noise corresponds to the measured temperature of black-body (MW absorbing foam) $T = 300$K and non-thermal noise corresponds to noise-equivalent temperature of $T_{\mathrm{NE}} = 53$ K. In this approach we consider the thermal signal as the proper result (fundamentally guaranteed by the theory of black-body radiation) and the non-thermal noise as a noise added by our device. However, if we were to measure another signal in relation to the thermal, the noise-equivalent temperature in the presented environment would be $T_{\mathrm{NE}} = 353$ K, as presented in the Sup. Tab. II, along with other values.

The lowest limit of 3.8K was obtained with an additional filtering incorporating an optical cavity, that on the one hand allowed for the conversion of thermal radiation from the whole bandwidth (the bandwidth of the cavity was 160 MHz versus 16 MHz of conversion bandwidth), and on the other hand allowed for successful filtration of wideband noise – the initial bandwidth that could couple to the signal fiber after passing through filters, at the order of 500 GHz (1.2 nm), was narrowed down to 160 MHz. This allowed for the elimination of noise, which we identified as 480nm-induced glass fluorescence, and led us to reducing noise-equivalent temperature of our device from 53K

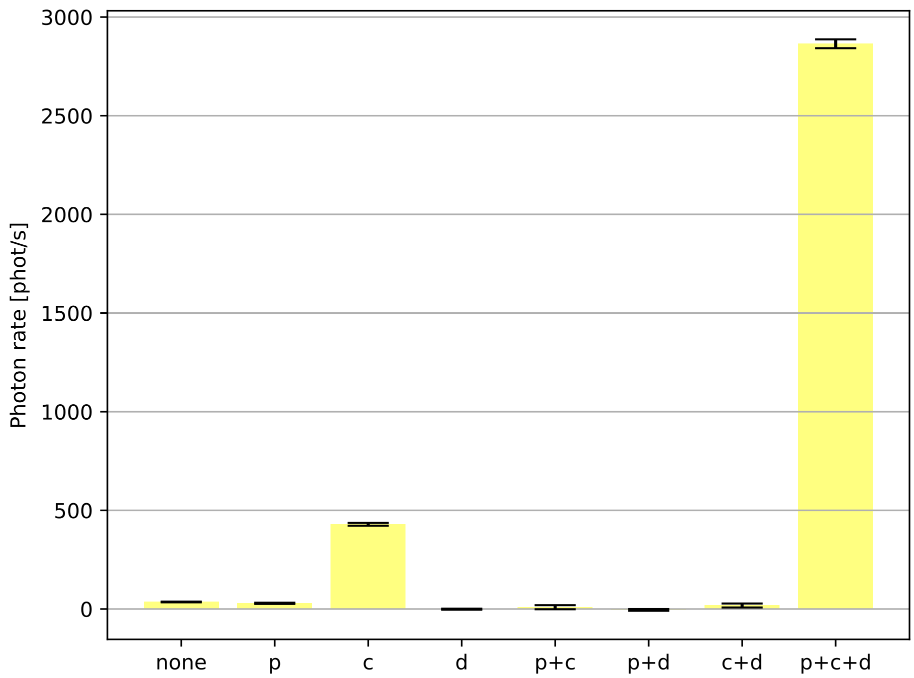

Supplementary Figure 4. Photon rate contributions for each field after introducing spectral filters. *p* – *probe* (780 nm), *c* – *coupling* (480 nm), *d* – *decoupling* (1258 nm). Again, the MW field has no effect on photon rates, apart from the case with all the other fields on. The error bars are calculated from the propagation of the standard deviation from the Sup. Fig. 3, where in each case $\bar{n}$ is explicitly noted as photon rates on the Y axis.

Source of signal	**Overall noise**	**Thermal noise**	**Non-thermal noise**	**Glass fluorescence noise**	**Other noise**	**Thermal level (theory)**	**Adjusted thermal level (theory)**	**Thermal level (experimental)**
photon rate [phot/s]	2050	1740	310	270	40	n/a	n/a	n/a
equivalent MW intensity [pW/m^2]	400	340	61	53	8	n/a	360	n/a
equivalent MW field [μV/cm]	5.50	5.07	2.13	1.98	0.78	n/a	5.23	n/a
MW field density [nVcm^{-1}(rad/s)$^{-1/2}$]	n/a	**0.48**	n/a	n/a	n/a	**1.64**	**0.495**	**1.59**
noise-equivalent temperature [K]	353	300	**53**	46	7	n/a	n/a	n/a
part of overall noise	100%	85%	15%	13%	2%	n/a	n/a	n/a

Supplementary Table II. Reference for registered noise components and derived thermal level.

to 3.8K by improving the thermal/non-thermal noise ratio. This is a demonstration of sensitivity of our device to photon-based MW measurements. One could imagine approaching single-photon operations e.g. on cosmic microwave background with such a device (still noisy but not impossible, and subject to further optimizations).

The values obtained for the measurements with additional cavity filtering were 325±8 phot/s for thermal photons and 4.2±0.5phot/s for other noise photons, resulting in overall $T_{\rm NE} = 3.8 \pm 0.5$ K noise-equivalent temperature.

Photon rates and photon pair rates

In the Fig. 3**c** (and similarly in the Fig. 3**b**) the value of total registered photon rate with antenna turned off is $\bar{n}_{\text{th}} + \bar{n}_{\text{noise}} = 1550$ phot/s, thus from the 85% proportion, the thermal photon rate is $\bar{n}_{\text{th}} = 1320$ phot/s. The source of losses in this case (comparing to 1740 phot/s at the Fig. 2) is different measurement scheme compared to that in the Fig. 2. Namely, we utilise two channels of single-photon detector to measure correlation between them, so we use 50:50 fiber splitter – thus there is fiber – splitter – two fibers connection versus fiber – fiber connection. Actually, there is a slight asymmetry introduced by the splitter, where we register 660 phot/s on one channel of the detector and 890 phot/s on the other in case of the antenna turned off. However, these rates are for single photons on each channel. The rate of correlation-measured excess bunched photon pairs (contributing to the peak e.g. in the Fig. 3**b**) in thermal radiation is around 20 pairs/h.

All of the values of $\bar{n}_{\text{th}}$ and $\bar{n}_{\text{coh}}$ were measured by measuring photon rates on the two channels of the photon detector. Actually, the measured quality is $\bar{n}_{\text{th}} + \bar{n}_{\text{coh}} + \bar{n}_{\text{noise}}$ but individual rates can be extracted from a separate measurement with antenna turned off (thus $\bar{n}_{\text{coh}} = 0$) and from the knowledge of thermal/non-thermal noise proportion.

S.3 DERIVATION OF THE FIELD SPECTRAL DENSITY OF THE MEASURED THERMAL RADIATION

As for the derivation of 480 $\text{pVcm}^{-1}(\text{rad/s})^{-1/2}$ from the Fig. 2**a**, the registered signal with antenna turned off is 2050 phot/s, as demonstrated in the Sup. Tab. II. From this we deduce that as thermal noise corresponds to 85% of the signal, it is at the level of 1740 phot/s. This consequently corresponds to a measured field of 5.07 μV/cm, as we describe in the Methods. However, this is thermal field integrated over whole conversion bandwidth, so we divide by the square root of integrally measured bandwidth ($17.8 \cdot 2\pi$ MHz, as described in the Methods) and arrive at the 480 $\text{pVcm}^{-1}(\text{rad/s})^{-1/2}$.

To achieve consistency between measured 480 $\text{pVcm}^{-1}(\text{rad/s})^{-1/2}$ and theoretically predicted 1.64 $\mu\text{Vcm}^{-1}(\text{rad/s})^{-1/2}$, we notice that the theory predicts thermal spectral density propagating in all directions, in both polarisations. However, in the *Phase matching* section in the Methods, and in the Extended Data Fig. 2, we show that our converter is sensitive mainly to one circular polarisation and quite directional – only 18% of whole spherical distribution is coupled to the device. In consequence only around 9% of all thermal radiation incident can couple to the converter. Adjusting for that property, we arrive at the value 1.59 $\mu\text{Vcm}^{-1}(\text{rad/s})^{-1/2}$, from experimental data, which is very near the theoretical prediction of 1.64 $\mu\text{Vcm}^{-1}(\text{rad/s})^{-1/2}$.

S.4 SUPPLEMENTARY DISCUSSION ON THE COHERENCE OF THE CONVERSION PROCESS

Unaffected coherent conversion on long timescales can be demonstrated with introducing two MW fields of slightly different frequencies at the input of the converter. The converted signal for both MW fields would in this case experience the same fluctuations and thus the phase difference between the two signals will be preserved.

To demonstrate the coherence of the conversion process, we apply simultaneously two near-optimal MW fields (generated from different VCOs synchronized with the same clock) of similar strengths, detuned by $3 \cdot 2\pi$ MHz, to the antenna. The spectrum of the conversion signal registered with heterodyne detection (Extended Data Fig. 1**g**) is presented in the Sup. Fig. 5. We then take parts of the spectrum corresponding to the registered signals and perform an estimation of cross-spectral density between them using Welch's method. Then by using a standard normalization to the geometrical mean of both signals' power spectral densities obtained with the same method, we arrive with coherence $\mathcal{C}$. The results are presented in the Sup. Fig. 6.

The coherence measurement ($\mathcal{C} = 0.88$ at zero frequency) corresponds very well with the theoretical limit based on the signal-to-noise ratio

$$\mathcal{C}_{\max} = \frac{\text{SNR}}{1 + \text{SNR}} \approx 0.89, \tag{4}$$

constituting a proof of nearly perfect coherence of the presented microwave-to-optical conversion process.

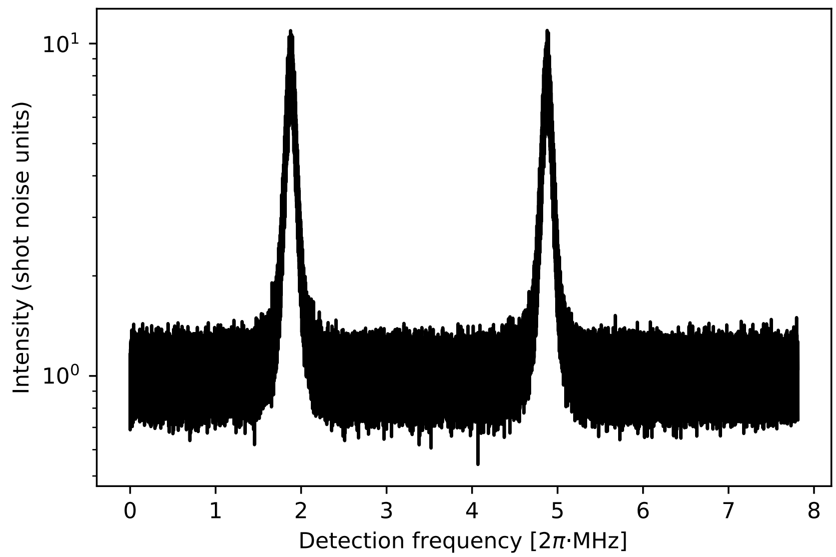

Supplementary Figure 5. The spectrum of two simultaneously converted MW signals in the heterodyne dection setup. The spectrum is averaged over 100 measurements. The intensity is normalized to the shot noise of the heterodyne. The signal-to-noise ratio is measured as SNR = 8.2 (9.2 dB).

S.5 MICROWAVE CONVERTER ACTING AS A MICROWAVE DETECTOR

The proposed scheme could work as a MW detector instead of converter, for example by employing shot-noise limited heterodyne detection with a local oscillator at the converted signal's wavelength. We present an exemplary result of this kind as a spectral characteristics of the output signal in the Extended Data Fig. 1**e** in the Methods. There we show the readout of a signal of around 2.9 mV/cm with SNR of 13.5 dB. As the signal have a bandwidth of 86 kHz, we may assume a phase noise compensation mechanism and that would yield us a sensitivity of around 2.8 μVcm^{-1}Hz$^{-1/2}$. This result would be comparable with standard Rydberg electrometric sensitivity but well below the superheterodyne state-of-the-art sensitivity.

However, photon-counting detection, for which the proposed scheme is suitable (and standard electrometric setups are not due to poor spectral separation of optical fields), entails new type of photonic operations and measurements that are not possible elsewhere, e.g. the presented autocorrelation measurement. These new types of measurements are not straightforwardly comparable to the heterodyne measurement, as here we are not subjected to the shot noise but, as we show, we hit the thermal noise limit (that has not been approached yet in heterodyne detection). In photon-counting detection the thermal limit is a limit not on the spectral sensitivity of the detection in [μVcm^{-1}Hz$^{-1/2}$] (as is the case for the shot noise limit in heterodyne detection) but for minimal detectable field in [μV/cm]. If we wanted to measure electric field using that method, we would arrive at minimal detectable field of 5.5 μV/cm, as presented in the Sup. Tab. II, with SNR of 1 in relation to thermal (and other) noise.

The wide operational bandwidth of the converter is the cause of high level of thermal noise that limits the sensitivity of the converter employed as an electrometric detector. We could imagine trading the bandwidth's figure of merit for the minimal detectable field, e.g. by directing the converted signal via a narrowband (20 kHz) tunable cavity – that would lead us to 170 nVcm^{-1} of thermal field. However, at this level of field we would expect count rate of only 2 phot/s, so it would require special care of other sources of noise. As the non-thermal noise registered with additional filtering translates to the level of 22 phot/s (as shown in the Fig. 2**a**), this would be the expected limit approached in this realization – resulting in 600 nVcm^{-1} of minimal detectable field.

A more concrete comparison, e.g. with the Ref. [47] is not straightforward, as the detection method is fundamentally different. In Ref. [47] a heterodyne detection is employed and the limit of the sensitivity – the noise floor – is given by atomic and technical noises, as claimed by the authors (we think that in most of the realizations the optical shot noise could also be an important contributing factor there), not the thermal radiation as in our case. Overall, this means that in homodyne/heterodyne detection quadrature operators of the field are measured ($\hat{X}$, $\hat{P}$), while in our work we use the photon-number operator $\hat{a}^\dagger\hat{a}$. We use photon counting, which is independent of the converted light

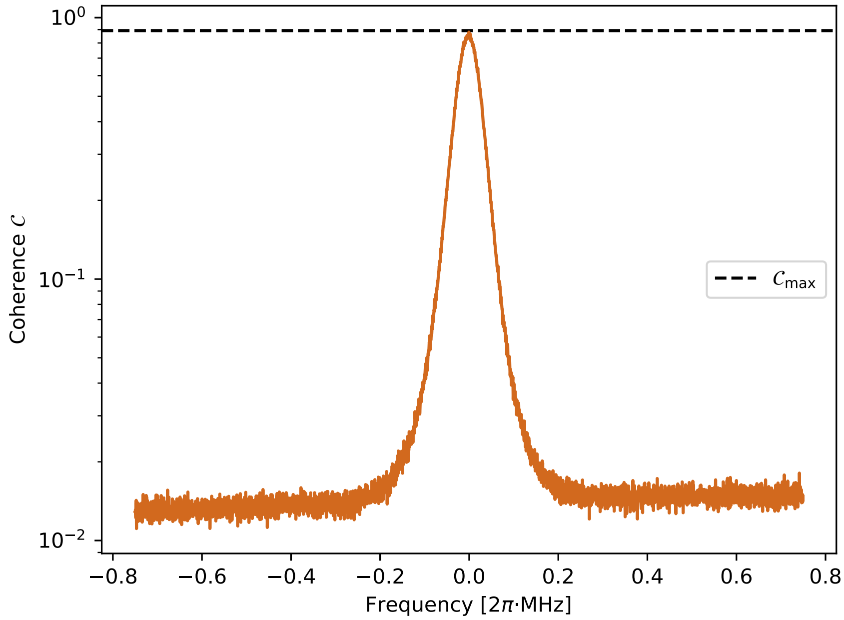

Supplementary Figure 6. The coherence of the conversion process, being the result of normalized cross-spectral density measurement performed on two MW signals converted simultaneously, in relation to the limit based on their signal-to-noise ratio. The result is averaged over 100 measurements.

frequency – registered photon counts from the thermal radiation correspond to the signal from the whole conversion bandwidth. This means that, when employing the converter as a field detector, the thermal limit is not a limit on sensitivity (in [μVcm^{-1}Hz$^{-1/2}$]) but rather on a minimal detectable field (in [μV/cm]), as the thermal radiation is integrated over the whole conversion bandwidth.

Regarding the operational dynamic range, e.g. in comparison to Ref. [47], in our setup we claim the lower limit of the converter's working range as the minimal detectable field given by the thermal radiation noise floor ($4{\cdot}10^{-10}$ W/m^2 in the Fig. 2), and the higher limit as >0.5 relative conversion efficiency ($2{\cdot}10^{-4}$ W/m^2) – this is 10 dB below the atomic saturation ($2{\cdot}10^{-3}$ W/m^2). The lower limit is dependent on the effective detection area, as well as the bandwidth of the conversion – the effective integration bandwidth of thermal radiation spectral density. We can envisage the filtering of the converted signal through a narrowband (e.g. 20 kHz) cavity. In that realization we would expect the detected thermal radiation to be at around 2 phot/s. Then other non-thermal noise at 22 phot/s (as shown in the Fig. 2**a**) would dominate the process, setting the minimal detectable field at $8{\cdot}10^{-12}$ W/m^2. That would result in 84 dB dynamic range (from the minimal detectable field to atomic saturation) and this result enables a fair comparison with the heterodyne detection device presented in the Ref. [47]. Though, in this case the instantaneous bandwidth of the conversion would of course be limited by the bandwidth of the mentioned narrowband cavity.

S.6 SUPPLEMENTARY DISCUSSION ON THE OPTICAL-TO-MICROWAVE CONVERSION

Demonstration of the reverse process of optical-to-microwave conversion is an important topic of research that has yielded solutions in different systems, Ref. [14, 18, 22, 28, 29, 31]. In our case the reverse conversion should also be possible, as confirmed by the model [Eq. (1)]. However, as the spontaneous emission branching ratios from the Rydberg states are not favorable, the emitted MW field would be very weak and difficult to detect in free space. A clear solution is to couple the atoms to a resonator which confines the MW field and enhances the decay rate on the MW transition.